RESEARCH ARTICLE

ADVANCED HEALTHCARE MATERIALS
www.advhealthmat.de

A Heparin-Functionalized Scaffold with HB-EGF Immobilization for Tissue Engineering

*Bowu Peng, Huajian Chen, Chengyu Lu, Tianjiao Zeng, Man Wang, Toru Yoshitomi, Naoki Kawazoe, Yingnan Yang, and Guoping Chen**

The introduction of growth factors (GFs) into scaffolds to mimic the in vivo microenvironment is a promising approach for tissue engineering. In this study, a heparin-functionalized scaffold is designed to mimic the GFs reservoir function of extracellular matrix (ECM). Owing to its heparin-binding domain, heparin-binding epidermal growth factor-like growth factor (HB-EGF) is effectively and spatially captured by heparin-functionalized scaffold. Furthermore, the strong interaction between heparin and heparin-binding domain confers excellent stability of the immobilized HB-EGF in scaffold over a long period. The heparin-functionalized scaffold immobilized with HB-EGF facilitates cell adhesion and promotes proliferation of human mesenchymal stem cells (hMSCs), while not inducing their differentiation during proliferation. These results indicate that the immobilized HB-EGF has a promotive effect on proliferation of hMSCs without triggering spontaneous differentiation, and the system shows as a promising strategy to enhance stem cells proliferation in scaffolds.

1. Introduction

Tissue engineering (TE) has attracted considerable attention as a promising strategy for regeneration of functional tissues and organs to treat human diseases and defects.[1–4] As a key element of TE, scaffolds provide structural support for cell adhesion and proliferation,[5] while offering a 3D space that mimics the in vivo extracellular microenvironment. Scaffolds should possess porous and interconnected architectures to facilitate cell distribution, migration, adhesion, and proliferation, which can even determine cellular fate during the process.[5–9]

Mesenchymal stem cells (MSCs) are an attractive cell source for TE due to their multipotent properties, including self-renewal, plasticity, and multilineage differentiation.[10,11] MSC-based TE requires expansion of MSCs to reach sufficient numbers because patient-derived MSCs are limited and decline with age, and their slow growth may impair therapeutic efficacy.[10,12,13] MSCs cultured in porous scaffolds can proliferate to large numbers and subsequentially differentiate into functional tissues. During this process, promotion of cell proliferation in the porous scaffolds is critical. One effective strategy to enhance cell proliferation is the incorporation of bioactive compounds or motifs into the porous structure.

Bioactive factors (BFs) are molecules that can interact with tissues and regulate cell functions, including growth factors (GFs), cytokines, and other biomolecules.[14,15] Among these, GFs have been most extensively studied in TE.[15,16] Despite their powerful therapeutic potential, their short half-life and low stability render the susceptibility of deactivation and degradation in biological microenvironments (e.g., enzymatic activity), which hinder their further clinical application.[17,18] The efficient delivery of GFs is essential for regulating cell functions, including migration, proliferation, survival, and differentiation, and thus plays a crucial role in tissue regeneration. Generally, physical (e.g., adsorption or entrapment) and chemical methods (e.g., covalent binding) are commonly employed to load GFs.[16,19,20] However, physical techniques often lead to burst and non-responsive release, while covalent bonding typically targets in amino groups, which may alter the bioactivity of GFs or cause effects distinct from those of free GFs.[21] Potential overdosing risks, non-responsive release, and bioactivity loss may further induce therapeutic side effects.[16] Consequently, new platforms are needed for efficient delivery of GFs. Bioaffinity-based methods and genetic engineering strategies are emerging as promising alternatives to sequester GFs and regulate cellular functions, thereby circumventing the drawbacks of conventional methods.[16,22–26]

The extracellular matrix (ECM) is a 3D network surrounding cells in vivo and composed of diverse macromolecules. It not only participates in cellular processes but also serves as a reservoir for

B. Peng, H. Chen, C. Lu, T. Zeng, M. Wang, T. Yoshitomi, N. Kawazoe, G. Chen
Research Center for Macromolecules and Biomaterials
National Institute for Materials Science
Ibaraki 305-0044, Japan
E-mail: Guoping.CHEN@nims.go.jp
B. Peng, C. Lu, T. Zeng, M. Wang, G. Chen
Graduate School of Science and Technology
University of Tsukuba
Ibaraki 305–8577, Japan
Y. Yang
Graduate School of Life and Environmental Science
University of Tsukuba
Ibaraki 305–8572, Japan

The ORCID identification number(s) for the author(s) of this article can be found under https://doi.org/10.1002/adhm.202502771

DOI: 10.1002/adhm.202502771

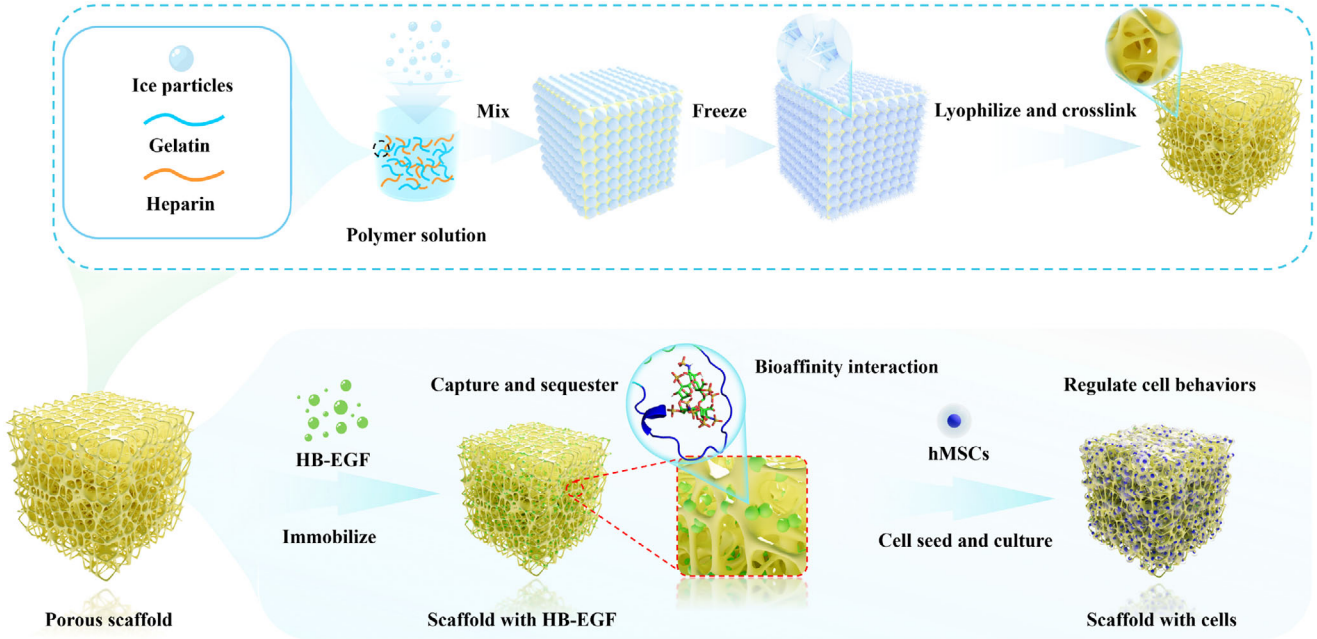

Figure 1. Schematic illustration of the design and preparation of the composite system comprising a porous gelatin/heparin scaffold and HB-EGF for tissue engineering.

GFs.[17] ECM contains abundant GFs such as insulin-like growth factor, fibroblast growth factor, hepatocyte growth factor and transforming growth factor-β. These GFs associate with ECM to maintain their activities and regulate cell functions such as rapid extracellular signaling activation, information transfer, function memory and matrix homeostasis.[27] Moreover, the activity of GFs immobilized by ECM can be controlled by this bioaffinity and result in a longer and localized signaling activation.[27] As a result, ECM-derived materials have been explored as ideal platforms for safe and economical delivery of GFs in TE.[28–30] Glycosaminoglycans (GAGs), along with their proteoglycan derivatives and glycoproteins, are key mediators of GFs sequestration within the ECM.[20,31] Heparin, a linear polysaccharide and member of the GAGs family, possesses the highest negative charge density of any naturally derived biomolecules. It has been extensively applied in TE and drug delivery as an effective candidate for GFs loading. Heparin functions as an affinity-binding molecule and has been shown to interact promiscuously with various GFs, thereby extending their half-lives and preserving bioactivity in biological microenvironments.[32–36] Heparin-binding epidermal growth factor-like growth factor (HB-EGF), a member of the epidermal growth factor (EGF) family, regulates MSCs migration, proliferation, survival, and differentiation.[37–39] HB-EGF contains both an EGF-like domain and a heparin-binding (HB) domain, conferring strong affinity for heparin or heparan sulfate. Gelatin, a hydrolyzed form of collagen, has also been widely used for scaffold preparation in 3D cell culture.[40–42]

Therefore, in this study, a gelatin/heparin (GH) porous scaffold was designed and prepared by using pre-prepared ice particles as a porogen reagent. HB-EGF was spatially sequestered within the GH porous scaffold through affinity-binding between its HB domain and heparin. The efficiency and stability of the immobilized HB-EGF in the GH scaffold were characterized, and its effects on proliferation and differentiation of MSCs were systematically evaluated.

2. Results

2.1. Preparation and Characterization of Scaffolds

The composite scaffold was prepared by immobilizing HB-EGF in the GH porous scaffold. At first, GH scaffold was fabricated by using ice particulates as a porogen reagent (**Figure 1**). Ice particulates with diameters between 150 – 250 μm were adopted to control the porous structure of the scaffold. The gelatin scaffold (G scaffold) without heparin was prepared as a control. The G and GH scaffolds exhibited similar porous structures, with large spherical pores containing small pores on the large pore walls, indicating that all the scaffolds possessed well-interconnected structures. In addition, the addition of heparin did not influence the microstructure of the scaffold (**Figure 2**a–d; Figure S1, Supporting Information). The size distribution of large spherical pores in G and GH scaffolds was 191.6 ± 26.6 μm and 193.3 ± 27.1 μm, respectively (Figure S2, Supporting Information). FT-IR (Figure S3, Supporting Information) showed the presence of amide A peak at 3300 cm^{-1}, representing the stretching frequency of N–H in amide groups. A strong amide II peak ≈ 1546 cm^{-1}, attributed to the bending frequency of N–H conjugated with C–O, was observed along with an amide I peak ≈ 1628 cm^{-1}, indicating the stretching vibration of C═O in amide groups. Peaks at 1105 and 983 cm^{-1} corresponded to the stretching frequency of S = O and S–O in heparin.[43] In the GH scaffold, the correlative peaks of S═O and S—O were observed ≈ 1120 and 973 cm^{-1}, confirming the successful conjugation between gelatin and heparin. The presence of heparin in the GH scaffold was further verified by Alcian blue staining.[44] The G scaffold

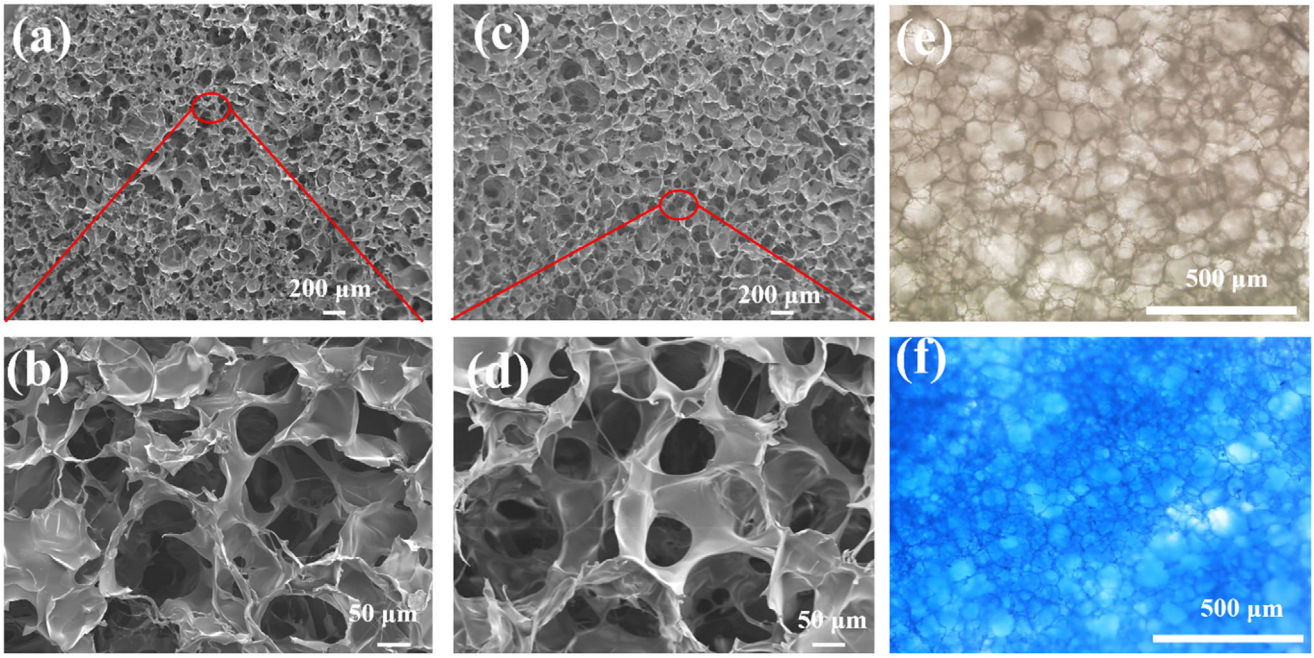

Figure 2. Microstructures of the scaffolds: Scanning electron microscopy (SEM) images of horizontal cross-sections of a,b) G scaffold and c,d) GH scaffold; Alcian blue staining of e) G scaffold and f) GH scaffold.

was not positively stained (Figure 2e), indicating the absence of heparin in the gelatin control. In contrast, the GH scaffold was positively stained (Figure 2f), and the homogeneity of staining indicated the homogeneous distribution of heparin throughout the GH scaffold (Figure 2f). Together, the Alcian blue staining and FT-IR results demonstrated hybridization of heparin and gelatin, confirming the successful preparation of GH scaffold.

The mechanical properties of dry and hydrated scaffolds were also measured (Figure S4, Supporting Information). The G and GH scaffolds had the same Young's modulus under both dry and hydrated conditions. However, the hydrated scaffolds showed much lower Young's modulus than the dry scaffolds. These results indicated that the addition of heparin did not influence the mechanical properties of porous scaffolds.

2.2. Immobilization of HB-EGF in GH Scaffold

Heparin is a type of GAGs with a high negative charge due to abundant carboxylic and sulfonate groups in its structure (**Figure 3**a).[45,46] HB-EGF, a member of the EGF family, contains a HB domain and an EGF-like domain (Figure 3b).[47,48] The HB domain of HB-EGF plays critical role in its immobilization. Analysis of the electrostatic potential of HB-EGF indicated that the HB domain carried a positive charge, enabling interaction with negatively charged heparin to form a stable complex through electrostatic and hydrogen-bonding interactions (Figure 3b; Figure S5, Supporting Information).[49,50] Docking analysis of heparin and HB-EGF (Figure 3c) showed that the recognition of heparin by HB-EGF occurred specifically in the HB domain of the protein, where hydrogen bonds were formed. Localization of formed hydrogen bonds between heparin and HB-EGF revealed the interactions were attributed to heparin-binding domain. These results demonstrated the essential role of heparin-binding domain in establishing a growth factor reservoir in this system.

The successful immobilization of HB-EGF in the GH scaffold was examined by immunochemical staining of HB-EGF. The G and GH scaffolds without HB-EGF were not positively stained (**Figure 4**a,d). The G scaffold incubated with HB-EGF solution showed slight staining, likely due to the physical absorption of HB-EGF (Figure 4b). In contrast, the GH scaffold immobilized with HB-EGF exhibited very strong staining (Figure 4e), indicating a large amount of HB-EGF was immobilized through the specific interaction between heparin and HB-EGF. The long-term retention of immobilized HB-EGF in the GH scaffold was further investigated. After incubation in PBS for 7, 14, and 21 days, immunochemical staining of the GH scaffold immobilized with HB-EGF remained strong (Figure 4f; Figure S6, Supporting Information), demonstrating that the immobilized HB-EGF in GH scaffold was stable and could be retained for extended periods. In comparison, the G scaffold coated with HB-EGF showed weakened staining after 7 days, indicating that the absorbed HB-EGF in the G scaffold was unstable and could be desorbed during incubation. Furthermore, ELISA analysis showed that the loading efficiency of HB-EGF in the GH scaffold was 92.6 ± 0.1%, which was comparable to the previously reported results.[51] Collectively, these findings demonstrated that the GH scaffold could significantly enhance the loading and retention of HB-EGF.

2.3. Cell Adhesion, Distribution, and Viability in Scaffolds

Next, hMSCs were seeded and cultured in the scaffolds. The cell seeding efficiency in the GH (-) (GH) and GH (+) (GH-

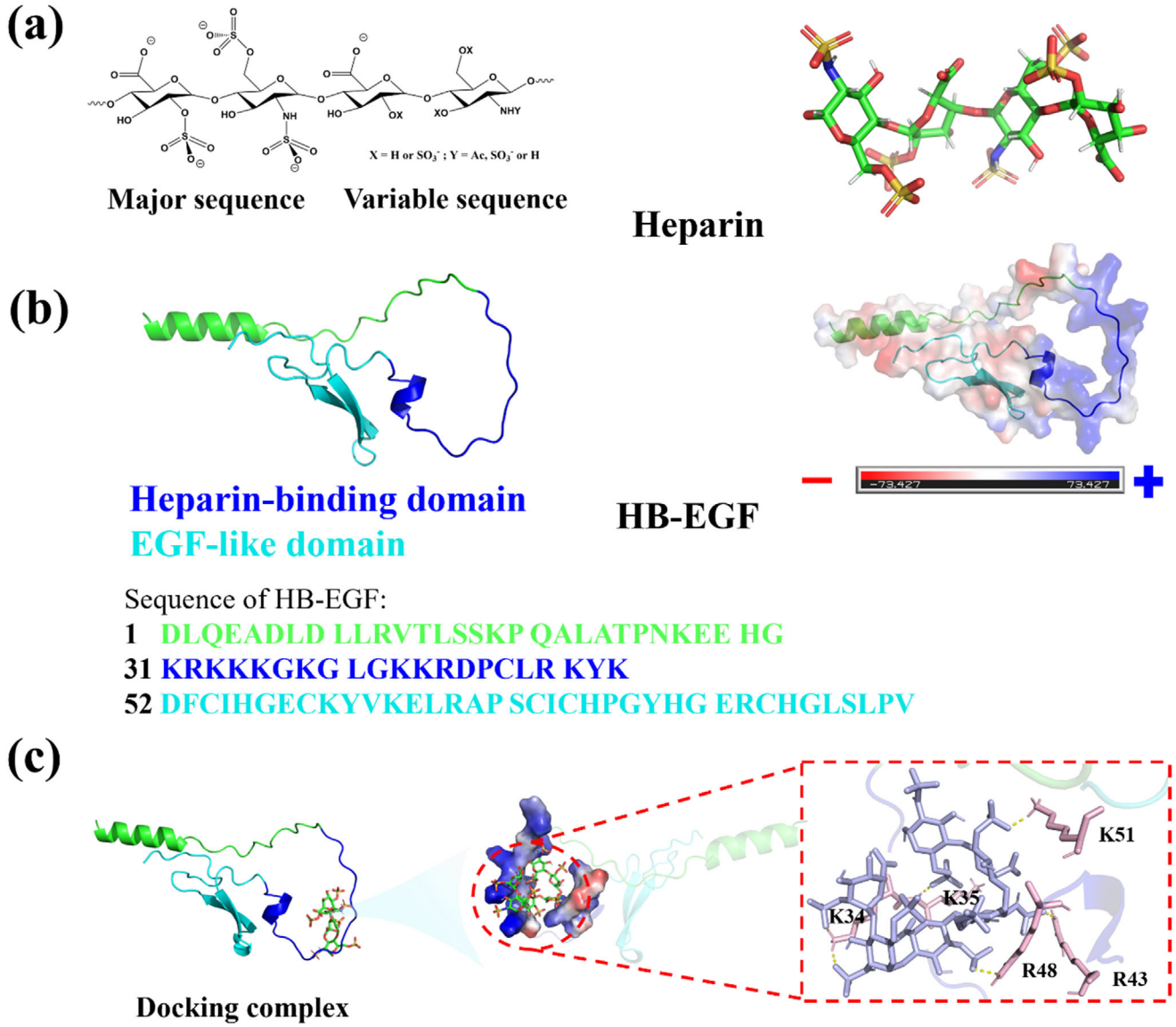

Figure 3. Structure of heparin and HB-EGF: a) Chemical and modeling structure of heparin; b) Modeling structure, electrostatic distribution and peptide sequence of HB-EGF and c) Interaction analysis of docking complex. Yellow dotted line: hydrogen bonds formed between heparin and HB-EGF.

HB-EGF) scaffolds was 96.3 ± 1.6% and 95.9 ± 1.1%, respectively (Table S1, Supporting Information). All scaffolds showed high seeding efficiency due to their interconnected microporous structures. As shown in **Figure** 5a,d, cells adhered to the surfaces of the interconnected pores in the GH and GH-HB-EGF scaffolds. The two scaffolds showed similar adhesion results, and the immobilized HB-EGF did not affect adhesion properties. After 7 days (Figure 5b,e) and 21 days (Figure 5c,f) of culture, more cells were observed in the pores of scaffolds compared to 1 day of culture. After 21 days of culture, more cells were observed in the GH-HB-EGF scaffolds than in the GH scaffolds, indicating cell proliferation in the scaffolds.

Cell distribution in the scaffolds was assessed by nucleus staining (Figure 5g–l). The nuclei were homogeneously stained from the top surface to the bottom of all scaffolds, showing uniform cell distribution in all scaffolds after 1 day of culture (Figure 5g–i). After 3 days, the cells remained homogeneously distributed in all scaffolds (Figure 5j–l), indicating that the immobilized HB-EGF did not affect cell distribution. The similar microporous structures of all scaffolds likely explained this observation. The high cell seeding efficiency and homogenous distribution of cells were ascribed to the well-interconnected porous structures of the scaffolds.

Cell viability in the scaffolds was investigated by live/dead staining (**Figure** 6a–f). Nearly all cells were alive after 1 day (Figure 6a–c) and 3 days (Figure 6d–f) of culture. Even after 7 and 21 days, almost all cells remined viable (Figure S7, Supporting Information). The cell density increased after 21 days of culture due to cell proliferation in the scaffolds. These results indicated that the cells maintained high viability and proliferated in all scaffolds.

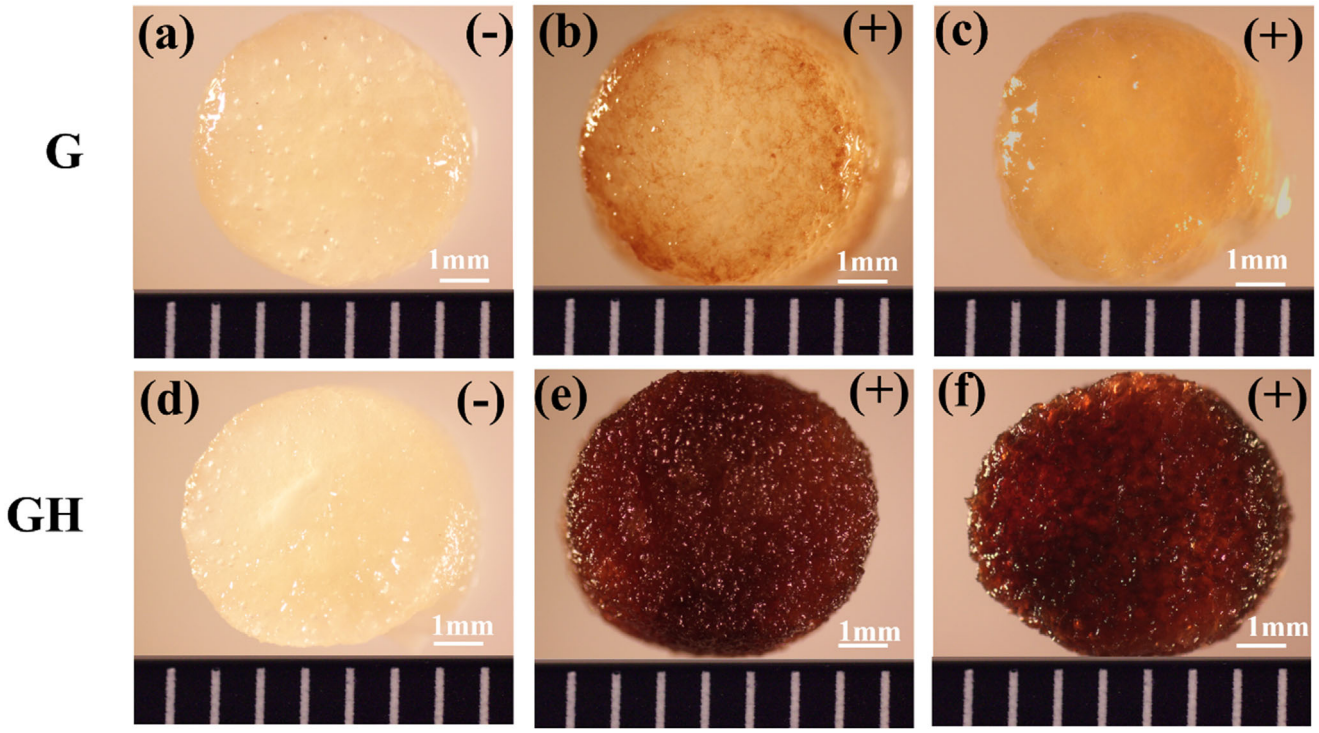

Figure 4. Immunochemical staining of the scaffolds. a) G scaffold without HB-EGF; b) G scaffold incubated with HB-EGF immediately after preparation; c) G scaffold incubated with HB-EGF after 7 days; d) GH scaffold without HB-EGF; e) GH scaffold immobilized with HB-EGF immediately after preparation; f) GH scaffold immobilized with HB-EGF after 7 days. (-): without HB-EGF; (+): with HB-EGF.

2.4. Effect of Immobilized HB-EGF on Cell Proliferation and Differentiation

Quantification of DNA amount (**Figure** 7a) was used to compare cell proliferation in the GH and GH-HB-EGF scaffolds. The DNA amount in GH-HB-EGF scaffolds was significantly higher than in GH scaffolds, suggesting that the GH-HB-EGF scaffolds enhanced cell proliferation more effectively. The immobilized HB-EGF could promote hMSCs proliferation during 3D culture in the porous scaffold. In addition, the effects of immobilized HB-EGF and free HB-EGF on proliferation enhancement of hMSCs were also evaluated (Figure S8, Supporting Information). Both the free and immobilized HB-EGF groups showed higher DNA amount than the group without HB-EGF. Compared with the free HB-EGF, the immobilized HB-EGF induced a more sustained proliferation enhancement of hMSC, likely due to its prolonged half-life and preserved bioactivity conferred by heparin binding, which may extend EGFR activation and thereby promote greater cellular proliferation.[51–53]

To evaluate the effects of immobilized HB-EGF on differentiation of hMSCs, chondrogenic differentiation was first investigated. The sGAG amount of hMSCs after 21 days of culture was measured (Figure 7b,c). The sGAG amount in both GH and GH-HB-EGF scaffolds increased over time. At each time point, the sGAG amount in the GH-HB-EGF scaffolds was significantly higher than in the GH scaffolds. However, the sGAG/DNA ratio, representing the sGAG production per cell, did not differ significantly between hMSCs cultured in the GH and GH-HB-EGF scaffolds (Figure 7c). These results indicated that hMSCs in both scaffolds had the same capacity for sGAG production. Thus, immobilized HB-EGF did not affect sGAGs synthesis.

Furthermore, expression of chondrogenic genes was analysed by RT-qPCR after hMSCs were cultured in the scaffolds for 3, 7, 14, and 21 days (Figure 7d–g). Four chondrogenic related genes, type I collagen (COL I), type II collagen (COL II), aggrecan (ACAN), and SRY-box transcription factor 9 (SOX 9), were selected for analysis. Expression levels of COL I, COL II, ACAN, and SOX 9 showed no significant difference between GH and GH-HB-EGF scaffolds at any time point. Moreover, the expression of COL II was very low. Collectively, these results indicated that the immobilized HB-EGF did not affect chondrogenic differentiation of hMSCs. Although the immobilized HB-EGF showed promotive effect on the proliferation of hMSCs during 3D culture in the porous scaffold, it had no influence on the chondrogenic differentiation of hMSCs.

And then, the effects of immobilized HB-EGF on osteogenic and adipogenic differentiation of hMSCs during 21 days of culture were also evaluated (Figure S9, Supporting Information). The osteogenesis-related genes, alkaline phosphatase (ALP) and runt-related transcription factor 2 (RUNX2), were used for evaluation of osteogenic differentiation. The adipogenesis-related genes, fatty acid binding protein-4 (FABP4) and lipoprotein lipase (LPL), were used for evaluation of adipogenic differentiation. The expression level of these genes in hMSCs cultured in GH-HB-EGF scaffolds was very low. These results indicated that the GH-HB-EGF did not induce osteogenic or adipogenic differentiation of hMSCs. Taken together, the findings demonstrated

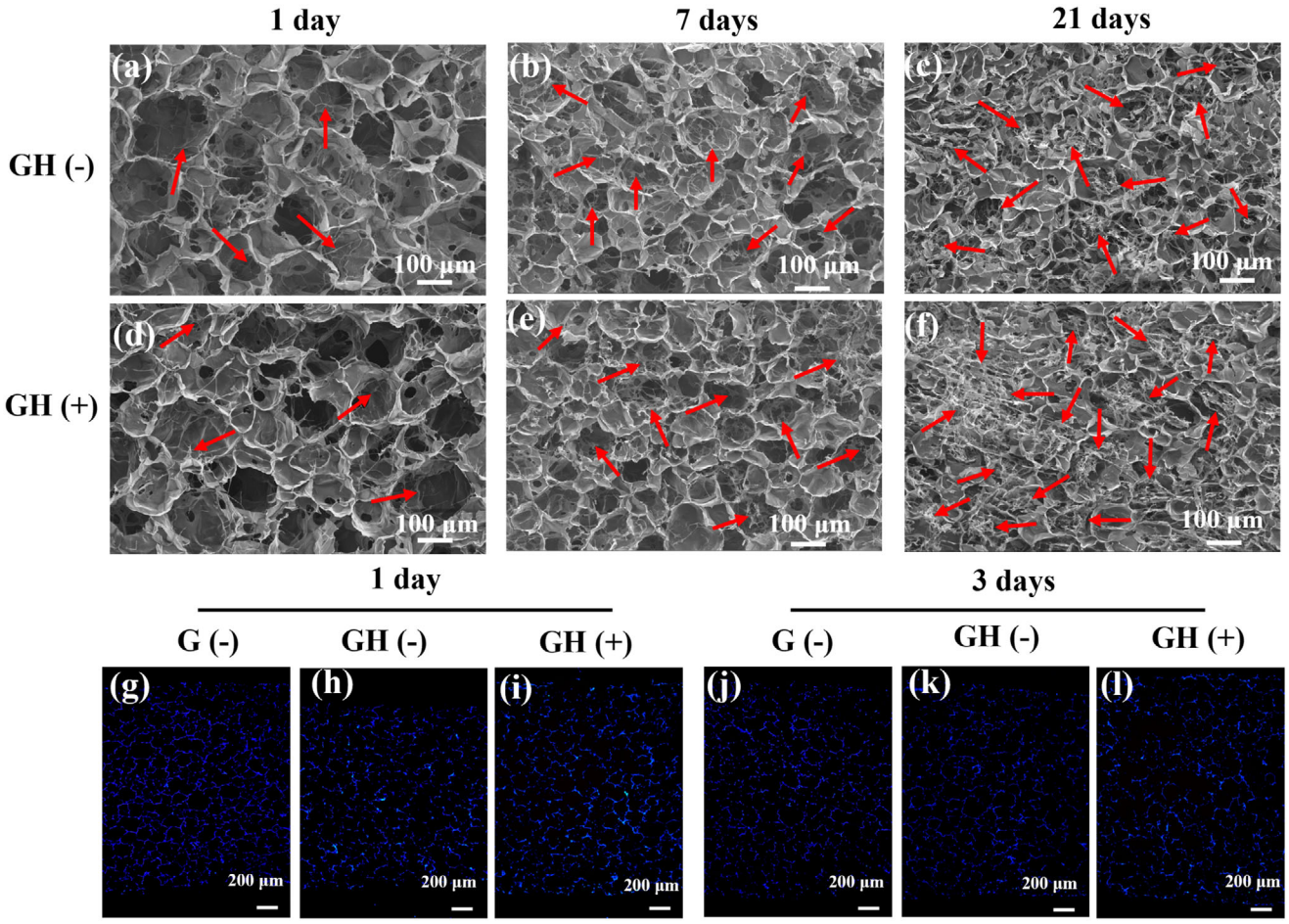

Figure 5. Cell adhesion and distribution in the scaffolds. a–f) SEM images of scaffolds after hMSCs were cultured for 1 day: a) GH (-) scaffold and d) GH (+) scaffold; 7 days: b) GH (-) scaffold and e) GH (+) scaffold; and 21 days: c) GH (-) scaffold and f) GH (+) scaffold. Arrows indicate the cells. g-l) Nucleus staining of hMSCs cultured in scaffolds for 1 day: g) G (-) scaffold, h) GH (-) scaffold and i) GH (+) scaffold; 3 days: j) G (-) scaffold, k) GH (-) scaffold and l) GH (+) scaffold. Blue fluorescence indicates cell nuclei. (-): without HB-EGF; (+): with HB-EGF.

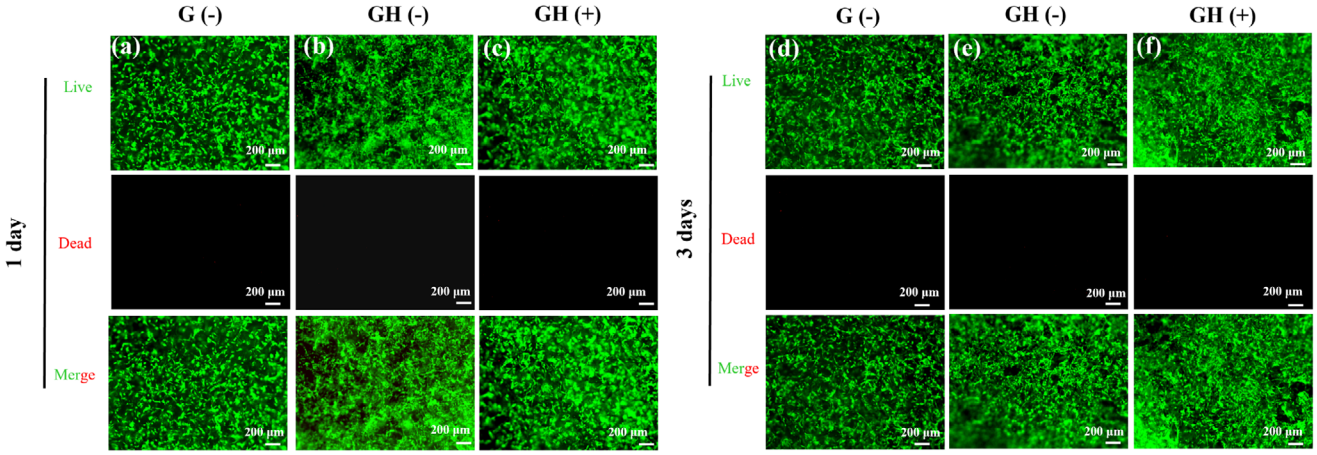

Figure 6. Cell viability in the scaffolds. Live/dead staining of hMSCs after 1 day of culture: a) G (-) scaffold, b) GH (-) scaffold and c) GH (+) scaffold; after 3 days of culture: d) G (-) scaffold, e) GH (-) scaffold and f) GH (+) scaffold. Green fluorescence indicates living cells while red fluorescence indicates dead cells. (-): without HB-EGF; (+): with HB-EGF.

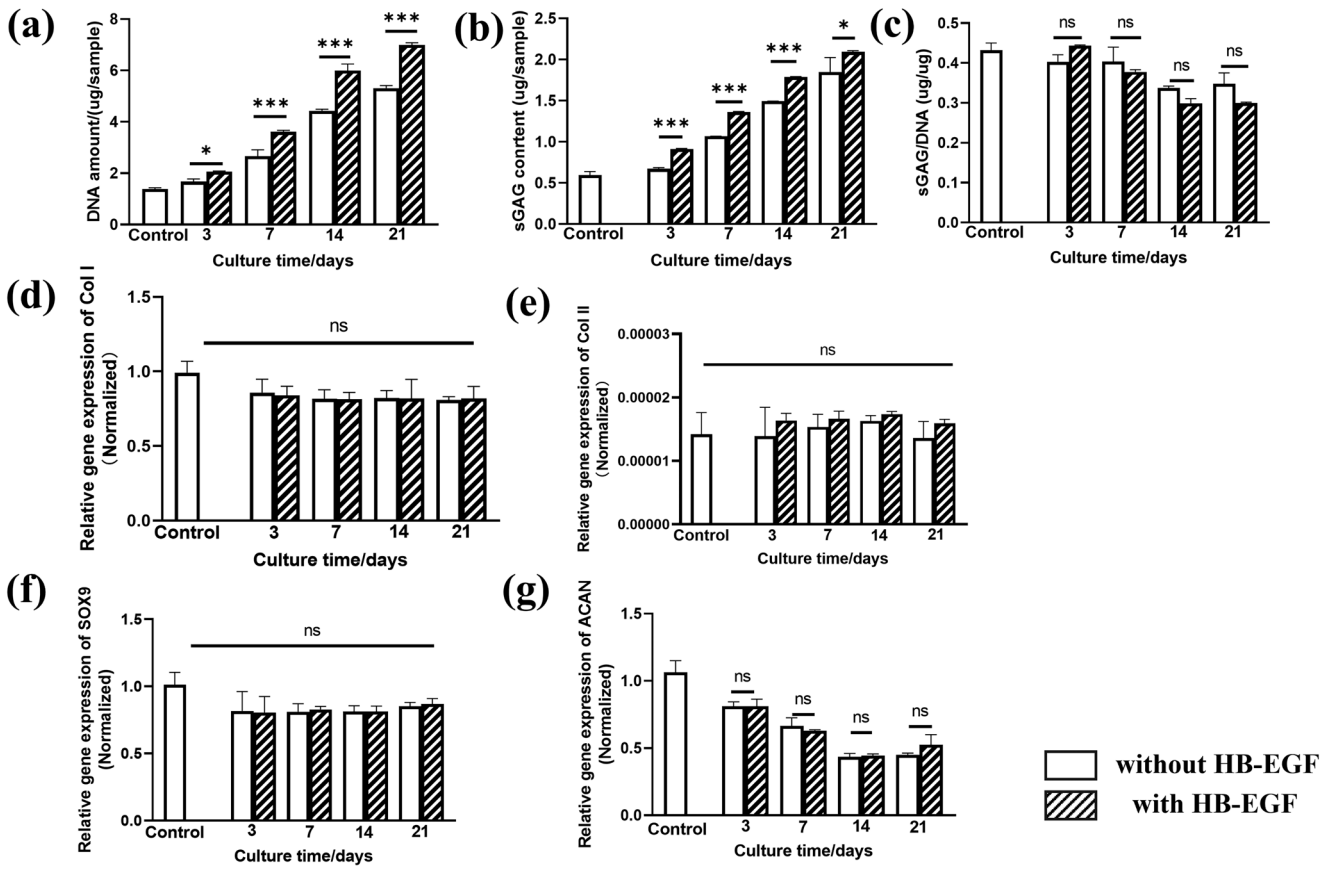

Figure 7. Proliferation and chondrogenic differentiation of hMSCs in the scaffolds. a) DNA quantification; and b) sulfated glycosaminoglycan (sGAG) quantification; c) sGAG/DNA ratio; d–g) Gene expression levels of COL I, COL II, SOX 9 and ACAN in hMSCs cultured in GH (-) and GH (+) scaffolds for 3, 7, 14, and 21 days. Data are presented as the mean ± SD ($n = 3$). Significant differences: $^{*}p < 0.05$; $^{**}p < 0.01$; $^{***}p < 0.001$; ns., not significant. (-): without HB-EGF; (+): with HB-EGF.

that the immobilized HB-EGF did not trigger chondrogenic, osteogenic or adipogenic differentiation of hMSCs.

2.5. In Vivo Efficacy and Biosafety Evaluation of Scaffolds

Subcutaneous implantation was performed to investigate the in vivo efficacy and biosafety of the scaffolds. The hMSCs were seeded in the GH scaffolds and GH-HB-EGF scaffolds and cultured for 3 days. The scaffolds were then subcutaneously implanted in the backs of nude mice for 10 days. The GH and GH-HB-EGF scaffolds were harvested and examined by live/dead staining and HE staining. The scaffolds shrank after 10 days of implantation (**Figure** 8a,b), likely due to suppression by surrounding tissues, as hydrated scaffolds had weak mechanical properties. Live/dead staining indicated that the cells in GH and GH-HB-EGF scaffolds remained viable (Figure 8c). HE staining showed that more cells were detected in the GH-HB-EGF scaffolds than in the GH scaffolds (Figure 8d). Furthermore, the major organs including heart, liver, spleen, lung and kidney from the mice implanted with GH-HB-EGF scaffolds, as well as from mice without implantation, were cross-sectioned and examined by HE staining. Gross appearance and histology showed no significant differences between the organs from the mice implanted with GH-HB-EGF scaffolds and the mice without implantation (Figure 8e; Figure S10, Supporting Information). These results demonstrated the in vivo efficacy and biological safety of the GH-HB-EGF scaffolds.

3. Discussions

In this study, the GH porous scaffold was prepared for immobilization of HB-EGF to generate GH-HB-EGF composite scaffold. Heparin in the GH scaffold specifically bound to the HB-EGF, resulting in a high loading efficiency of HB-EGF in the GH scaffold. The immobilized HB-EGF was retained in the scaffold for a long period due to the stable bioaffinity binding between heparin and HB-EGF. More importantly, the extended half-life and preserved bioactivity of immobilized HB-EGF, provided through heparin interaction, allowed more efficient and economical use of HB-EGF in biomedical applications.

The immobilized HB-EGF promoted the proliferation of hMSCs but did not induce their differentiation. These findings were consistent with the previous results of free HB-EGF on the functions of MSCs.[37,39] Previous studies have reported that HB-EGF binds to EGFR (HER1), which subsequently result in phosphorylation of tyrosine residues in the receptor kinase domain, thereby activating the downstream Akt and Erk1/2 pathways to regulate

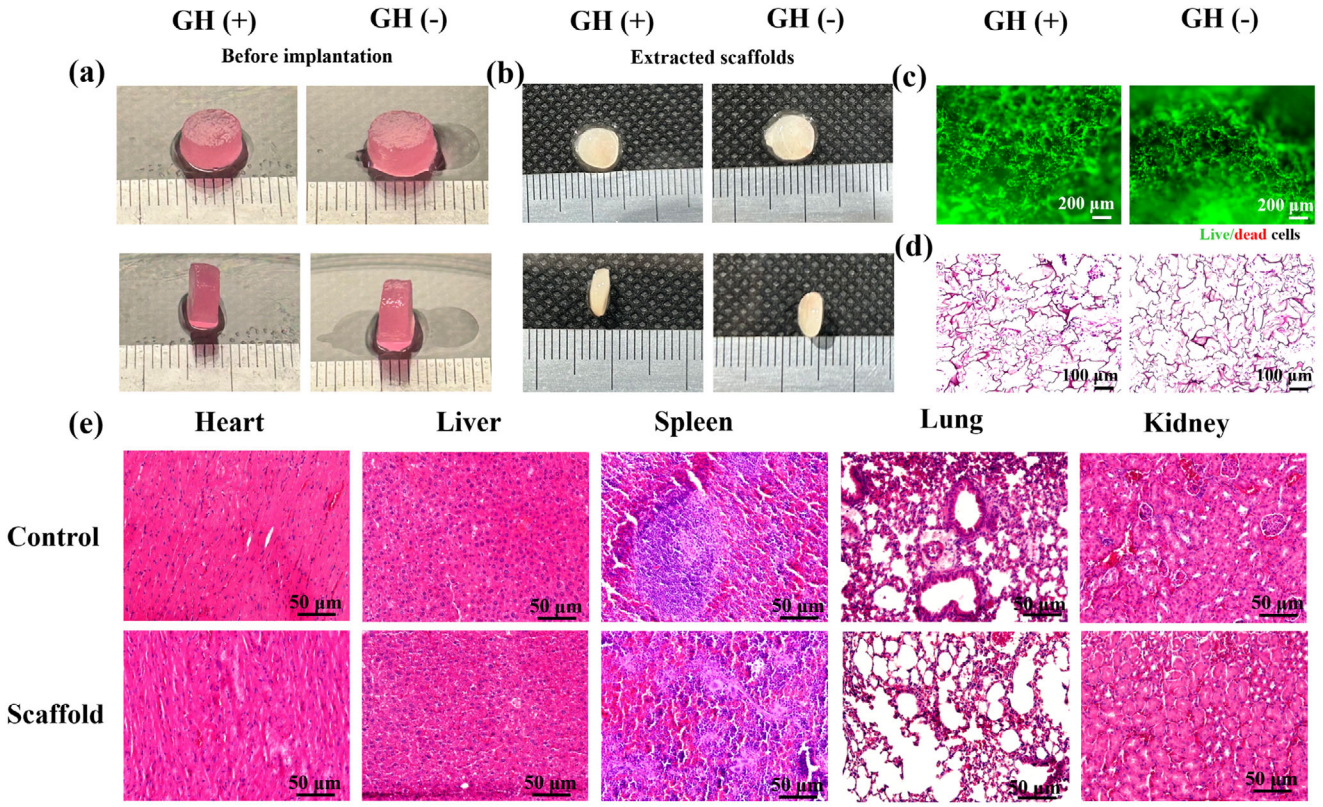

Figure 8. In vivo efficacy and biosafety of scaffolds. a) Gross appearance of scaffolds before implantation; b) Gross appearance of implants after 10 days implantation; c) Live/dead staining of implants; d) HE staining of implants; e) HE staining of heart, liver, spleen, lung and kidney from the mice without or with cell/scaffold implantation for 10 days. (-): without HB-EGF; (+): with HB-EGF.

cells proliferation.[48,54,55] Additionally, HB-EGF has been shown to inhibit spontaneous chondrogenic, osteogenic and adipogenic differentiation of MSCs.[37,39,56] This inhibitory effect on differentiation is temporary and reversible, depending on the presence and dosage of HB-EGF.[37] The preliminary treatment with HB-EGF is necessary to hamper the differentiation cascade and the block effect disappears after removal of HB-EGF.[37] During this process, HB-EGF-mediated suppression of MSCs differentiation likely occurs through inhibition of BMP-Smad1/5/8 signalling,[39] and the BMP-Smad1 pathway plays a critical role in osteoblast and chondrocyte differentiation.[57–60] The efficacy and biosafety of this system were also explored in vivo, and the results demonstrated the potential of this design for future clinical application.

In this study, we only investigated the effects of immobilized HB-EGF on human bone marrow-derived MSCs. The effects of immobilized HB-EGF on other types of stem cells, such as adipose-derived MSCs, require further investigation. Nevertheless, immobilization of HB-EGF in GH scaffold proved to be a useful method for maintaining the bioactivity of growth factors and promoting proliferation of stem cells during 3D culture in porous scaffolds, which is a critical process for TE. Furthermore, there are other BFs that, similar to HB-EGF, interact with heparin, and their bioactivities may also be enhanced by forming heparin-BF complexes.[61,62] The system developed in this study may therefore offer broader and multifunctional applications in TE.

4. Conclusion

GH scaffolds were prepared by an ice particulates method to mimic the growth factor reservoir function of the ECM. The porous structure was controlled by ice particulates, and the scaffold featured large spherical pores with good interconnectivity. The addition of heparin significantly enhanced the binding capacity and stability of HB-EGF in the scaffold, resulting in the formation of GH-HB-EGF scaffold. The prepared GH-HB-EGF scaffold supported efficient cell seeding, homogenous cell distribution, and enhanced proliferation of hMSCs, while not inducing their differentiation. Therefore, this system is expected to serve as a base platform for introducing bioactive factors into porous scaffolds for TE applications.

5. Experimental Section

Materials: Gelatin (type B from bovine skin) and heparin-binding epidermal growth factor-like growth factor (HB-EGF) were purchased from Sigma–Aldrich. Heparin sodium, 1-ethyl-3-(3-dimethylaminopropyl) carbodiimide (EDC), N-hydroxysuccinimide (NHS), acetic acid and ethanol were obtained from Wako Pure Industries, Ltd. All reagents were used directly unless otherwise indicated.

Preparation of Gelatin/Heparin (GH) and Gelatin (G) Scaffolds: The GH porous scaffold was prepared by an ice particulates-based method according to the previous work[6,63,64] with some changes. Briefly, ice particulates were acquired by spraying pure water into liquid nitrogen and the ice particulates with diameters of 150–250 μm were sieved in a low tempera-

ture chamber. Then, the gelatin and heparin sodium were dissolved in 35% (v/v) acetic acid solution, respectively and the two solutions were mixed to form the homogeneous solution which contained 8% (m/v) gelatin and 0.4% (m/v) heparin sodium. Subsequently, the temperature of the mixture solution and ice particulates were balanced at −4 °C for 6 h. And then, the ice particulates were added into the mixture solution at a ratio of 7 (ice):3 (solution) (m/v) and the final mixture was transferred into a silicon mold. The construct was placed in a −80 °C freezer for 12 h for freezing. Finally, the frozen construct was lyophilized and crosslinked with a series of ethanol solutions containing EDC and NHS. After cross-linking, the scaffold was washed with MilliQ water to obtain the GH composite scaffold. A control G scaffold without heparin was also prepared by the same method.

Microstructure Characterization and Heparin Staining: The microstructures of scaffolds were evaluated by scanning electron microscopy (SEM, JSM-IT800, Tokyo, Japan). The pore sizes of the scaffolds were measured by using an ImageJ software to calculate the average diameters of 100 pores from each of three SEM images. The heparin in the scaffolds was stained according to a previously reported method.[44] Briefly, the gelatin/heparin composite scaffold and gelatin control scaffold were treated with Alcian Blue 8GX (0.5% w/v) in 3% acetic acid for 30 min and washed by MilliQ water for three times. And then, the stained samples were lyophilized and characterized by an optical microscope.

Characterization of Mechanical Property of Scaffolds: The mechanical property of scaffolds was evaluated by Young's modulus of scaffolds. The scaffolds were punched into cylinder with a diameter of 6 mm and thickness of 6 mm. The Young's modulus of the scaffolds was measured in both dry and hydrated status. The hydrated scaffolds were prepared by immersing the scaffolds into PBS for 2 h at room temperature. The samples were compressed at 0.1 mm s^{-1} by texture analyzer (TA, XTPlus. Texture Technologies, Hamilton, MA, USA). The initial linear region of the stress-strain curves was chosen to calculate the Young's modulus, and three samples from each group were investigated for the evaluation.

HB-EGF Immobilization and Evaluation—HB-EGF Immobilization: The G and GH scaffolds were punched into cylinder discs (φ 6 × 3 mm), and the discs were sterilized with 70% (v/v) ethanol aqueous solution for 30 min. After washing with sterilized MilliQ water for 3 times, the scaffold discs were immersed in HB-EGF solution (100 ng mL^{-1}) under shaking at 4 °C for 24 h. And then, the treated scaffolds were washed by sterilized PBS for 3 times and stored at −20 °C for further use.

HB-EGF Immobilization and Evaluation—Immunochemical Staining of HB-EGF: Firstly, the GH scaffolds immobilized with HB-EGF were incubated in PBS containing 2% bovine serum albumin 4 °C for overnight for non-specific antigen blocking. After that, the scaffolds were incubated with anti-HB-EGF primary antibody (Human HB-EGF Antibody, AF-259-NA, biotechne R&D SYSTEM) at 4 °C for overnight. After three PBS washes, samples were incubated with the Donkey Anti-Goat IgG H&L at room temperature for 2 h, followed by three further PBS washes. Color development was performed with 3, 3- diaminobenzidine (DAB) for 5 min, and samples were characterized by an optical microscopy. The control G scaffold that was incubated with HB-EGF (100 ng mL^{-1}, 4°C, 24 h) and washed with PBS was used to assess HB-EGF adsorption.

HB-EGF Immobilization and Evaluation—Loading Efficiency of HB-EGF: Residual HB-EGF solution and PBS eluates from immobilization and washing were collected and HB-EGF concentration in the collected solution was measured by an ELISA test (Human HB-EGF Quantikine ELISA Kit, biotechne R&D SYSTEM). The immobilized amount of HB-EGF in the scaffolds was calculated by subtracting the residual HB-EGF amount from the initial input. The loading efficiency was calculated by dividing the immobilized amount of HB-EGF in the scaffolds with input amount. Quadruplicate samples were analyzed to calculate the mean values and standard deviations.

HB-EGF Immobilization and Evaluation—Stability of Immobilized HB-EGF: The G and GH scaffolds incubated with HB-EGF were placed in PBS under shaking (60 rpm) at 37 °C for 7 days to assess the stability of immobilized HB-EGF. The PBS was replaced with fresh solution every 3 days. After 7 days, scaffolds were collected and evaluated by immunochemical staining of HB-EGF. To evaluate longer term stability, GH scaffold samples were also examined after 14 and 21 days.

Computational Modeling of Heparin and HB-EGF—Modeling of Heparin: The heparin model was generated by GLYCAM Web Tools (http://glycam.org).

Computational Modeling of Heparin and HB-EGF—Modeling of HB-EGF: Modeling of HB-EGF was based on the peptide sequences of HB-EGF[47,49] and constructed with SWISS-MODEL.[65–69] Electrostatic potential distribution of HB-EGF was calculated by PyMOL software (The PyMOL Molecular Graphics System, Version 2.6 Schrödinger, LLC).

Computational Modeling of Heparin and HB-EGF—Molecular Docking of Heparin and HB-EGF: Pre-processing of docking was based on an AutoDockTools[70] and binding of heparin to HB-EGF was analyzed by an AutoDock.[71,72,70,73] The semi-flexible docking was used in the docking process. Heparin was treated as a completely flexible part and HB-EGF as a rigid part.[50] The coordinates of the central grid point of maps were defined as follows: $x = -30.277$, $y = -8.034$, $z = 38.953$ and the grid spacing was 0.375 Å. The Lamarckian genetic algorithm with an initial population size of 300 and a termination condition of 27 000 generations and 2.5×10^7 energy evaluations were used. A total of 50 independent runs were carried out.

Cell Culture and Functional Evaluations—Culture of hMSCs in Scaffolds: The scaffold discs (φ 6 × 3 mm) were sterilized with a 70% (v/v) ethanol aqueous solution for 30 min and rinsed with sterilized MilliQ water for 3 times. Human bone-marrow-derived mesenchymal stem cells (hMSCs) at passage 2 obtained from Lonza (Walkersville MD, USA) were subcultured in MSCGM medium. The hMSCs after two passages were collected by trypsin treatment and resuspended in culture medium at a cell concentration of 5×10^6 cells mL^{-1}. A total of 84 µL cell suspensions were added onto the top side of the scaffold discs and cultured for 6 h. After 6 h culture, the scaffold discs were turned upside down and the other side was also seeded with another 84 µL cell suspensions. After an additional 6 h, samples were transferred to flasks containing DMEM (2.5% FBS, 4mM L-Glutamine, and 100 U mL^{-1} Penicillin-Streptomycin) for continuing culture under shaking at 60 rpm. During cell seeding, the unadhered MSCs in the seeding medium were collected and counted for calculation of seeding efficiency. For cells cultured in GH scaffold with immobilized HB-EGF, the concentration of HB-EGF in the culture system was 25 ng mL^{-1}.

Cell Culture and Functional Evaluations—Evaluations of hMSCs Adhesion, Viability, Distribution and Proliferation: The hMSCs cultured in scaffolds for 1, 7, and 21 days were observed by SEM. Briefly, the scaffolds were washed with PBS and fixed with 2.5% glutaraldehyde for 1h. After fixation, the scaffolds were washed with MilliQ water and lyophilized. The lyophilized scaffolds were coated with platinum for SEM observation. Live/dead staining was conducted for evaluating cell viability and nuclei staining was conducted to examine cell distribution in the scaffolds. After culture for 1 and 3 days, the cells were stained by using a Live/dead cell staining kit and Hoechst 33258. The stained samples were observed by a fluorescence microscope.

Cell Culture and Functional Evaluations—Evaluation of Immobilized HB-EGF and Free HB-EGF on hMSCs Proliferation: The hMSCs were seeded in G and GH-HB-EGF scaffolds at equal densities. The cell-G scaffolds were divided into two groups: G scaffold without HB-EGF and G scaffold supplemented with free HB-EGF. The concentration of HB-EGF in free and immobilized groups was designed at 25 ng mL^{-1}. After 7 days of culture, three groups were collected, and DNA amount was measured. Triplicate samples were used for each measurement.

Cell Culture and Functional Evaluations—Quantification of DNA and Sulfated Glycosaminoglycan (sGAG): Proliferation of hMSCs in scaffolds was evaluated by quantifying the DNA amount. GH scaffolds without HB-EGF were used as a control. The cell/scaffold constructs after cell seeding and culture for 3, 7, 14 and 21 days were harvested for quantification of DNA and sGAG amounts. The harvested samples were washed, freeze-dried and digested with papain solution at 60 °C under shaking for 12 h. The papain solution was prepared by dissolving papain in 0.1M PBS buffer (400 µg mL^{-1}) with L-cysteine hydrochloride monohydrate (5 mM) and EDTA (5 mM) at a pH of 6. The amount of DNA and sGAG in the digestion solution was quantified with Hoechst 33258 and a BlyscanTM Glycosaminoglycan Assay Kit, respectively. Triplicate samples were analyzed to calculate the mean values and standard deviations.

Real-Time PCR: Samples cultured for 3, 7, 14, and 21 days were collected for analysis of gene expression. The hMSCs cultured in the GH scaffolds without HB-EGF were used as a control. Samples were washed three times with PBS and frozen in liquid nitrogen. The frozen samples were pulverized with a crusher and lysed with a Sepasol-RNA I Super G solution (1 mL). Total RNA was extracted according to a reported protocol.[74] After reverse transcription with a high-capacity cDNA reverse transcription kit, amplification of glyceraldehyde-3-phosphate dehydrogenase (GAPDH, housekeeping gene), collagen type I (Col1a2), collagen type II (Col2a1), aggrecan (ACAN) and SOX9 was conducted with a QuantStudio 3 Real-Time PCR System (Thermo Fisher Scientific). The previously reported primer and probe sequences as shown below were used.[75,76] GAPDH: (forward) 5′-ATGGGGAAGGTGAAGGTCG-3′, (reverse) 5′-TAAAAGCAGCCCTGGTG-ACC-3′, (probe) 5′-CGCCCAATACGACCAAATCCGTTGAC-3′; Col1a2: (forward) 5′-CAGCCGCTTCACCTACAGC-3′, (reverse): 5′-TTTTGTATT-CAATCACTGTCTTGCC-3′, (probe): 5′−CCGGTGTGACTCGTGCAGCCATC-3′; Col2a1: (forward) 5′GGCAATAGCAGGTTCACGTACA-3′, (reverse) 5′-CGATAACAGTCTTGCCCCACTT-3′, (probe) 5′−CCGGTATGTTTCGTG-CAGCCATCCT-3′; ACAN: (forward) 5′-TCGAGGACAGCGAGGCC-3′, (reverse) 5′-TCGAGGGTGTAGCGTGTAGAGA-3′, (probe) 5′-ATGGAAC-ACGATGCCTTTCACCACGA-3′; SOX9: (forward) 5′-CACACAGCTCACTCG-ACCTTG-3′, (reverse) 5′-TTCGGTTATTTTTAGGATCATCTCG-3′, (probe) 5′-CCCACGAAGGGCGACGATGG-3′. For adipogenic differentiation, primer and probe sequences were used: *FABP4* (Hs00609791_m1, Lot: 1909263, Applied Biosystems), and *LPL* (Hs00173425_m1, Lot: 1953315, Applied Biosystems); For osteogenic differentiation, primer and probe sequences were used: *ALPL* (Hs01029144_m1, Lot: 2103375, Applied Biosystems) and *RUNX2* (Hs00231692_m1, Lot: 2080647, Applied Biosystems). A $2^{-\Delta\Delta Ct}$ method was used to calculate the relative expression of each gene with endogenous control (GAPDH). Expression levels were normalized against those of control group. Triplicate samples were analyzed to calculate the mean values and standard deviations.

Subcutaneous Implantation: All in vivo experiments were conducted with the approval from the Ethical Committee of Animal Experiments of NIMS (accreditation No: 76-2023-12) and according to the Committee Guidelines. hMSCs seeded scaffolds cylinders (φ 6 × 3 mm) of GH and GH-HB-EGF were cultivated in vitro for 3 days before implantation. Nude mice obtained from Charles River Laboratories (Yokohama, Japan) were used for subcutaneous implantation. The mice were sacrificed to collect the samples and organ tissues after 10 days ($n = 3$). The samples collected were washed with PBS 3 times and fixed with 10% neutral buffered formalin for 24 h at room temperature. The fixed samples were dehydrated, embedded in paraffin and sliced with microtome to obtain slice with a thickness of 5 µm. The slices were stained with HE and evaluated by optical microscopy.

Statistical Analysis: The quantitative data were statistically analyzed by one-way analysis of variance (ANOVA) with Tukey's post hoc test using GraphPad Prism software (GraphPad Software, Boston, Massachusetts USA, www.graphpad.com). The data are shown as the mean ± standard deviations (S.D.) ($n = 3$) and significant differences are expressed as * ($p < 0.05$), ** ($p < 0.01$), and *** ($p < 0.001$).

Supporting Information

Supporting Information is available from the Wiley Online Library or from the author.

Acknowledgements

This work was supported by JSPS KAKENHI Grant Number 24K03289 and JST SPRING Grant Number JPMJSP2124.

Conflict of Interest

The authors declare no conflict of interest.

Data Availability Statement

The data that support the findings of this study are available from the corresponding author upon reasonable request.

Keywords

HB-EGF, heparin, hMSCs, immobilization, porous scaffold, tissue engineering

Received: June 2, 2025
Revised: September 19, 2025
Published online:

[1] A. Atala, *Tissue Eng., Part A* **2024**, *30*, 5.
[2] M. Risbud, *Biogerontology* **2001**, *2*, 117.
[3] J. F. Mano, R. L. Reis, *J. Tissue. Eng. Regen. Med.* **2007**, *1*, 261.
[4] C. W. Patrick Jr, *Anat. Rec.* **2001**, *263*, 361.
[5] Q. L. Loh, C. Choong, *Tissue Eng., Part B* **2013**, *19*, 485.
[6] Q. Zhang, H. Lu, N. Kawazoe, G. Chen, *Acta Biomater.* **2014**, *10*, 2005.
[7] Z.-Z. Zhang, D. Jiang, J.-X. Ding, S.-J. Wang, L. Zhang, J.-Y. Zhang, Y.-S. Qi, X.-S. Chen, J.-K. Yu, *Acta Biomater.* **2016**, *43*, 314.
[8] I. Bružauskaitė, D. Bironaitė, E. Bagdonas, E. Bernotienė, *Cytotechnology* **2016**, *68*, 355.
[9] A. Di Luca, K. Szlazak, I. Lorenzo-Moldero, C. A. Ghebes, A. Lepedda, W. Swieszkowski, C. Van Blitterswijk, L. Moroni, *Acta Biomater.* **2016**, *36*, 210.
[10] A. Caplan, *J. Pathol.* **2009**, *217*, 318.
[11] N. W. Marion, J. J. Mao, In *Methods in Enzymology*, Academic Press, Cambridge, Massachusetts **2006**, pp. 339–361.
[12] Y.-L. Si, Y.-L. Zhao, H.-J. Hao, X.-B. Fu, W.-D. Han, *Ageing Res. Rev.* **2011**, *10*, 93.
[13] M. S. Choudhery, M. Badowski, A. Muise, J. Pierce, D. T. Harris, *J. Transl. Med.* **2014**, *12*, 8.
[14] D. E. Discher, D. J. Mooney, P. W. Zandstra, *Science* **2009**, *324*, 1673.
[15] X. Tang, H. Qin, X. Gu, X. Fu, *Biomaterials* **2017**, *124*, 78.
[16] T. Chen, Y. Jiang, J.-P. Huang, J. Wang, Z.-K. Wang, P.-H. Ding, *J. Controlled Release* **2024**, *368*, 97.
[17] , *Handbook of the Extracellular Matrix: Biologically-Derived Materials*, (Eds: F. R. Maia, J. M. Oliveira, R. L. Reis), Springer International Publishing, Berlin, Germany **2024**.
[18] F.-M. Chen, M. Zhang, Z.-F. Wu, *Biomaterials* **2010**, *31*, 6279.
[19] D. Enriquez-Ochoa, P. Robles-Ovalle, K. Mayolo-Deloisa, M. E. G. Brunck, *Front. Bioeng. Biotechnol.* **2020**, *8*, 620.
[20] S. P. B. Teixeira, R. M. A. Domingues, M. Shevchuk, M. E. Gomes, N. A. Peppas, R. L. Reis, *Adv. Funct. Mater.* **2020**, *30*, 1909011.
[21] M. Rodrigues, H. Blair, L. Stockdale, L. Griffith, A. Wells, *Stem. Cells* **2013**, *31*, 104.
[22] A. C. Mitchell, P. S. Briquez, J. A. Hubbell, J. R. Cochran, *Acta Biomater.* **2016**, *30*, 1.
[23] B. Shan, F. Wu, *Adv. Mater.* **2024**, *36*, 2210707.
[24] H. Lu, N. Kawazoe, T. Kitajima, Y. Myoken, M. Tomita, A. Umezawa, G. Chen, Y. Ito, *Biomaterials* **2012**, *33*, 6140.
[25] H. Deng, F. Wang, Y. Zhou, H. Lei, H. Zhou, S. Chen, Z. Meng, M. He, D. Tu, H. Wang, X. Li, Q. Xia, X. Li, F. Wang, *Bioact. Mater.* **2025**, *52*, 511.
[26] F. Wang, A. Ning, X. Sun, Y. Zhou, H. Deng, H. Zhou, S. Chen, M. He, Z. Meng, Y. Wang, H. Xia, X. Ma, Q. Xia, *Biomaterials* **2025**, *316*, 122986.
[27] J. Taipale, J. Keski-Oja, *FASEB J.* **1997**, *11*, 51.
[28] E. D. F. Ker, B. Chu, J. A. Phillippi, B. Gharaibeh, J. Huard, L. E. Weiss, P. G. Campbell, *Biomaterials* **2011**, *32*, 3413.

[29] A. A. Golebiowska, J. T. Intravaia, V. M. Sathe, S. G. Kumbar, S. P. Nukavarapu, *Bioact. Mater.* **2024**, *32*, 98.
[30] H. Vilaça-Faria, J. Noro, R. L. Reis, R. P. Pirraco, *Bioact. Mater.* **2024**, *34*, 494.
[31] B. Mulloy, C. C. Rider, *Biochem. Soc. Trans.* **2006**, *34*, 409.
[32] D. B. Pike, S. Cai, K. R. Pomraning, M. A. Firpo, R. J. Fisher, X. Z. Shu, G. D. Prestwich, R. A. Peattie, *Biomaterials* **2006**, *27*, 5242.
[33] J. M. Wu, Y. Y. Xu, Z. H. Li, X. Y. Yuan, P. F. Wang, X. Z. Zhang, Y. Q. Liu, J. Guan, Y. Guo, R. X. Li, H. Zhang, *J. Mater. Sci.: Mater. Med.* **2011**, *22*, 107.
[34] J. Lee, J. J. Yoo, A. Atala, S. J. Lee, *Acta Biomater.* **2012**, *8*, 2549.
[35] D. Hachim, T. E. Whittaker, H. Kim, M. M. Stevens, *J. Controlled Release* **2019**, *313*, 131.
[36] Y. Ikegami, H. Mizumachi, K. Yoshida, H. Ijima, *Regener. Ther.* **2020**, *15*, 236.
[37] M. Krampera, A. Pasini, A. Rigo, M. T. Scupoli, C. Tecchio, G. Malpeli, A. Scarpa, F. Dazzi, G. Pizzolo, F. Vinante, *Blood* **2005**, *106*, 59.
[38] D. J. Watkins, Y. Zhou, C.-L. Chen, A. Darbyshire, G. E. Besner, *J. Surg. Res.* **2012**, *177*, 359.
[39] P. Li, Q. Deng, J. Liu, J. Yan, Z. Wei, Z. Zhang, H. Liu, B. Li, *J. Bone Miner. Res.* **2019**, *34*, 295.
[40] G. Lindberg, A. Norberg, B. Soliman, T. Jüngst, K. Lim, G. Hooper, J. Groll, T. Woodfield, *Front. Biomater. Sci.* **2024**, *3*, 1331032.
[41] A. B. Rashid, N.-N. Showva, M. E. Hoque, *Curr. Opin. Biomed. Eng.* **2023**, *26*, 100452.
[42] S. Afewerki, A. Sheikhi, S. Kannan, S. Ahadian, A. Khademhosseini, *Bioeng. Transla. Med.* **2019**, *4*, 96.
[43] I. Kim, S. S. Lee, S. Bae, H. Lee, N. S. Hwang, *Biomacromolecules* **2018**, *19*, 2257.
[44] N. Adhirajan, R. Thanavel, N. Naveen, T. S. Uma, M. Babu, *Polym. Bull.* **2014**, *71*, 1015.
[45] R. Linhardt, S. Murugesan, J. Xie, *CTMC* **2008**, *8*, 80.
[46] T. Liu, Y. Liu, Y. Chen, S. Liu, M. F. Maitz, X. Wang, K. Zhang, J. Wang, Y. Wang, J. Chen, N. Huang, *Acta Biomater.* **2014**, *10*, 1940.
[47] S. Higashiyama, K. Lau, G. E. Besner, J. A. Abraham, M. Klagsbrun, *J. Biol. Chem.* **1992**, *267*, 6205.
[48] D. T. Dao, L. Anez-Bustillos, R. M. Adam, M. Puder, D. R. Bielenberg, *Am. J. Pathol.* **2018**, *188*, 2446.
[49] G. Raab, M. Klagsbrun, *Biochimica et Biophysica Acta (BBA) – Rev. Cancer.* **1997**, *1333*, F179.
[50] S. Thönes, S. Rother, T. Wippold, J. Blaszkiewicz, K. Balamurugan, S. Moeller, G. Ruiz-Gómez, M. Schnabelrauch, D. Scharnweber, A. Saalbach, J. Rademann, M. T. Pisabarro, V. Hintze, U. Anderegg, *Acta Biomater.* **2019**, *86*, 135.
[51] N. R. Johnson, Y. Wang, *J. Controlled Release* **2013**, *166*, 124.
[52] G. S. Schultz, A. Wysocki, *Wound. Repair. Regen.* **2009**, *17*, 153.
[53] R. O. Hynes, *Science* **2009**, *326*, 1216.
[54] M. Rodrigues, L. G. Griffith, A. Wells, *Stem. Cell. Res. Ther.* **2010**, *1*, 32.
[55] L. A. Orofiamma, D. Vural, C. N. Antonescu, *Biochimica et Biophysica Acta (BBA) – Mol. Cell Res.* **2022**, *1869*, 119359.
[56] J. S. Lee, J. M. Suh, H. G. Park, E. J. Bak, Y.-J. Yoo, J.-H. Cha, *Differentiation* **2008**, *76*, 478.
[57] K. N. Retting, B. Song, B. S. Yoon, K. M. Lyons, *Development* **2009**, *136*, 1093.
[58] V. S. Salazar, L. W. Gamer, V. Rosen, *Nat. Rev. Endocrinol.* **2016**, *12*, 203.
[59] T. Katagiri, T. Watabe, *Cold. Spring. Harb. Perspect. Biol.* **2016**, *8*, a021899.
[60] D. Rigueur, S. Brugger, T. Anbarchian, J. K. Kim, Y. Lee, K. M. Lyons, *J. Bone Miner. Res.* **2015**, *30*, 733.
[61] M. Ishihara, S. Nakamura, Y. Sato, T. Takayama, K. Fukuda, M. Fujita, K. Murakami, H. Yokoe, *Molecules* **2019**, *24*, 4630.
[62] E. Nazarzadeh Zare, D. Khorsandi, A. Zarepour, H. Yilmaz, T. Agarwal, S. Hooshmand, R. Mohammadinejad, F. Ozdemir, O. Sahin, S. Adiguzel, H. Khan, A. Zarrabi, E. Sharifi, A. Kumar, E. Mostafavi, N. H. Kouchehbaghi, V. Mattoli, F. Zhang, V. Jucaud, A. H. Najafabadi, A. Khademhosseini, *Bioact. Mater.* **2024**, *31*, 87.
[63] S. Chen, Q. Zhang, T. Nakamoto, N. Kawazoe, G. Chen, *Tissue Eng., Part C* **2016**, *22*, 189.
[64] R. Sun, H. Chen, J. Zheng, T. Yoshitomi, N. Kawazoe, Y. Yang, G. Chen, *Adv. Healthcare. Mater.* **2023**, *12*, 2202604.
[65] N. Guex, M. C. Peitsch, T. Schwede, *Electrophoresis* **2009**, *30*, S162.
[66] M. Bertoni, F. Kiefer, M. Biasini, L. Bordoli, T. Schwede, *Sci. Rep.* **2017**, *7*, 10480.
[67] G. Studer, C. Rempfer, A. M. Waterhouse, R. Gumienny, J. Haas, T. Schwede, *Bioinformatics* **2020**, *36*, 1765.
[68] A. Waterhouse, M. Bertoni, S. Bienert, G. Studer, G. Tauriello, R. Gumienny, F. T. Heer, T. A. P. de Beer, C. Rempfer, L. Bordoli, R. Lepore, T. Schwede, *Nucleic Acids Res.* **2018**, *46*, W296.
[69] S. Bienert, A. Waterhouse, T. A. P. de Beer, G. Tauriello, G. Studer, L. Bordoli, T. Schwede, *Nucleic. Acids. Res.* **2017**, *45*, D313.
[70] G. M. Morris, R. Huey, W. Lindstrom, M. F. Sanner, R. K. Belew, D. S. Goodsell, A. J. Olson, *J. Comput. Chem.* **2009**, *30*, 2785.
[71] G. M. Morris, D. S. Goodsell, R. S. Halliday, R. Huey, W. E. Hart, R. K. Belew, A. J. Olson, *J. Comput. Chem.* **1998**, *19*, 1639.
[72] R. Huey, G. M. Morris, A. J. Olson, D. S. Goodsell, *J. Comput. Chem.* **2007**, *28*, 1145.
[73] S. Forli, R. Huey, M. E. Pique, M. F. Sanner, D. S. Goodsell, A. J. Olson, *Nat. Protoc.* **2016**, *11*, 905.
[74] E. A. Makris, A. H. Gomoll, K. N. Malizos, J. C. Hu, K. A. Athanasiou, *Nat. Rev. Rheumatol.* **2015**, *11*, 21.
[75] Y. Xie, L. Sutrisno, T. Yoshitomi, N. Kawazoe, Y. Yang, G. Chen, *Biomed. Mater.* **2022**, *17*, 034103.
[76] H. Lu, T. Hoshiba, N. Kawazoe, I. Koda, M. Song, G. Chen, *Biomaterials* **2011**, *32*, 9658.